

AN ATLAS OF H α AND R IMAGES AND RADIAL PROFILES OF 29 BRIGHT ISOLATED SPIRAL GALAXIES

REBECCA A. KOOPMANN

Union College and

Department of Physics and Astronomy, Schenectady, NY 12308

JEFFREY D. P. KENNEY

Astronomy Department and

Yale University, P.O. Box 208101, New Haven, CT 06520-8101

Accepted by *Astrophysical Journal*, 2005 September 2

ABSTRACT

Narrow-band H α +[NII] and broadband R images and surface photometry are presented for a sample of 29 bright ($M_B < -18$) isolated S0-Scd galaxies within a distance of 48 Mpc. These galaxies are among the most isolated nearby spiral galaxies of their Hubble classifications as determined from the Nearby Galaxies Catalog (Tully 1987a).

Subject headings: galaxies: spiral, galaxies: star formation, galaxies: fundamental parameters, galaxies: structure

1. INTRODUCTION

How does the environment of a galaxy influence its evolution? Finding an answer to this question requires extensive comparisons between galaxies in different environments, including those in the most isolated environments.

Many studies have sought to compare the global star formation properties of galaxies in field and cluster environments (see, for example, references in Koopmann & Kenney 2004a and a review by Poggianti 2005). The selection of isolated comparison samples in these studies is as important as the selection of the primary objects of study. In the case of a study on environmental effects, the comparison sample should ideally be made up of galaxies completely isolated from their surroundings. However, the distribution of galaxies in space appears to be strongly clustered, with few, if any, objects outside gravitationally associated structures. A truly isolated galaxy may not exist (e.g., Vettolani *et al.* 1986, Tully 1987b). All is not lost, however. The main requirement for a galaxy to serve as a comparison object in a study of the environmental effects on bright cluster galaxies is that it have a low probability of interaction with another galaxy of similar mass or with a group environment over a Hubble time. Such galaxies are not typical (since 69% of galaxies are located in groups; Tully 1987b), but they do exist.

We undertook to observe a sample of isolated galaxies as part of a study to compare the star formation properties of nearly 100 bright isolated and Virgo Cluster spiral galaxies via broadband R and H α images. We sought the most isolated nearby galaxies for our comparison sample, using the environmental information in the Nearby Galaxies Catalog (Tully 1987a, hereafter NBG). Because we wished to compare Virgo and isolated spirals as a function of Hubble type classification, we selected our sample based on Hubble type as well as local galaxy density, observing roughly equal numbers of different spi-

ral types, with luminosities, distances, and inclinations as similar as possible to those of Virgo spirals. We use the term ‘isolated’ for this sample rather than the more general term ‘field’. The selection of field samples is generally not subject to the stringent requirements outlined here, and many field galaxy samples contain group members.

Since our primary motivation was to find an isolated sample suitable for comparison to Virgo Cluster galaxies, our selection process was somewhat different from that of other studies which have sought to identify and characterize the most isolated galaxies. Studies such as Karachentseva (1973) and Pisano, Wilcots, & Liu (2002) apply more stringent density limitations, but their samples contain relatively few early-type spiral galaxies and are on average further away. We note that much larger samples of isolated galaxies are being compiled through studies such as Allam *et al.* (2005), who identify a sample of 2980 isolated galaxies in the Sloan Digital Sky Survey (SDSS; York *et al.* 2000) Data Release 1. The galaxies identified in this survey are on average at much greater distance than Virgo, but the sample contains a significant number of early-type galaxies.

A dilemma in selecting isolated galaxies for comparison was deciding whether or not to select only galaxies which had previous measurements at other wavelengths. For example, it would be useful to have a comparison sample of galaxies also mapped in HI and CO. However, we decided that such a selection criterion might bias the sample, since galaxies with mapped HI and CO were often selected because of their peculiarities. Our final sample contains rather obscure galaxies, but we hope that this will be changed in the future by further observations of these galaxies.

In this paper, we present images and radial profiles in H α and R for 29 isolated spiral galaxies. There are several other papers in this series. R and H α images and selection details of the Virgo Cluster sample are presented in Koopmann, Kenney, & Young (2001). Comparisons between the R and H α radial profiles of Virgo Cluster and isolated spirals are presented in Koopmann & Ken-

ney (1998; 2004a, 2004b).

This paper is organized as follows. The selection of the isolated galaxies is described in Section 2. Section 3 describes the observations and reduction procedures. Section 4 presents the atlas of isolated galaxies, including images and surface photometry.

2. SAMPLE SELECTION

An isolated comparison sample of galaxies should resemble the cluster sample as much as possible in distance and absolute magnitude, but be located in the lowest density regions possible. The selection of isolated galaxies was based on the environmental information contained in the NBG, supplemented by group listings from the work of Gourgoulhon *et al.* (1992).

The NBG lists 2367 galaxies with recessional velocities $< 3000 \text{ km s}^{-1}$. The catalog is essentially complete for galaxies with recessional velocities $< 1500 \text{ km s}^{-1}$. The galaxies in the catalog are assigned memberships within hierarchical structures ranging from large-scale ‘clouds’ to associations and groups. Associated galaxies must meet a critical density requirement to be considered a bound group with a crossing time shorter than a Hubble time. Unbound ‘associations’ of galaxies meet a density requirement one order of magnitude lower than the group requirement. Our first step towards finding the most isolated galaxies was to eliminate all group members, which amounts to approximately 69% of the NBG (Tully 1987b). The remaining galaxies were either in associations (20%) or ‘at-large’ within a cloud, i.e., apparently unassociated with other cloud members (10%). Selection of our sample from these galaxies was based on the Hubble type, local density, distances, recessional velocities, inclinations, and luminosities provided in the catalog (described in detail by Tully 1988).

We selected only spiral galaxies with Hubble types S0-Scd, and sought to observe sufficient galaxies of each spiral type to provide a comparison sample for Virgo Cluster galaxies. Thus the observed galaxies do not represent the actual number distribution in terms of Hubble type. Only galaxies with inclinations of $< 75^\circ$ were selected. The luminosity cutoff was set to the same as that of the Virgo Cluster sample: $M_B < -18$. The local density, distance, and recessional velocity limits were determined by experimentation to obtain sufficient numbers of early-type spirals, which are less common in field environments. To select galaxies with distances comparable to Virgo, a cutoff in velocity of 2500 km s^{-1} and a cutoff in distance of 33 Mpc (as listed by NBG) were applied. 66% ($\frac{19}{29}$) of the galaxies have $v_{\text{los}} < 1500 \text{ km s}^{-1}$ and 86% ($\frac{25}{29}$) $< 2000 \text{ km s}^{-1}$. Galaxies with $v_{\text{los}} > 1500 \text{ km s}^{-1}$ are mostly early-type spirals. The distances of the galaxies, originally extracted from the NBG, were reevaluated using the heliocentric velocity and the multiattractor model for the velocity fields within the Local Supercluster (Tonry *et al.* 2000; Masters, K. L., private communication), with an assumed Hubble constant of $70 \text{ km s}^{-1} \text{ Mpc}^{-1}$, 37% of the galaxies are within 20 Mpc, while 62% are within 25 Mpc.

Our absolute density cutoff was set at 0.3 gal Mpc^{-3} . The local density of a particular galaxy is based on the contributions of all galaxies with absolute magnitudes brighter than -16, including the galaxy itself. Local den-

sities range from $0.06 \text{ gal Mpc}^{-3}$ for an isolated galaxy to 4.2 gal Mpc^{-3} in the central regions of the Virgo Cluster. For comparison, the density of the Local Group is $0.52 \text{ gal Mpc}^{-3}$. The local density is at least 0.1 gal Mpc^{-3} for 90% of the galaxies of all classes, meaning that almost all galaxies have companions within $\sim 1 \text{ Mpc}$. (It should be emphasized that the Nearby Galaxies Catalog is not able to identify galaxies with small companions, i.e., companions with $M_B > -16$. However, our objective is to select galaxies which are the least likely to have experienced similar mass interactions.) In the observed sample, 69% of the 29 galaxies selected from the Nearby Galaxies Catalog have local densities $\leq 0.2 \text{ gal Mpc}^{-3}$ and $34\% \leq 0.1 \text{ gal Mpc}^{-3}$. 67% of the sample galaxies appear to belong to a specific cloud, but are ‘at-large’ in the cloud, and 33% belong to associations within clouds.

A total of 115 isolated galaxies matching our selection criteria were found in the NBG. We provide in Table 1 a summary of the percentages of galaxies observed, according to the classifications given by the two main catalogs: (i) *Revised Shapley Ames Catalog* (Sandage & Tammann 1987; hereafter RSA) or the *Carnegie Atlas* (Sandage & Bedke 1994; hereafter CA) and (ii) *Third Reference Catalog* (deVaucouleurs *et al.* 1991; hereafter RC3). (Note that only 86/115 of the NBG galaxies appeared in the RSA/CA.)

Additional targets were identified from a list of 86 isolated galaxies derived from analyses described in Gourgoulhon *et al.* (1992) and Fouqué *et al.* (1992) and kindly provided to us by P. Fouqué. The list is derived from a sample of 4143 galaxies with blue isophotal diameters, D_{25} , larger than $100''$ and recessional velocities $< 6000 \text{ km s}^{-1}$, with completeness of 84%. Group and association members were identified in a manner similar to the NBG, but with a somewhat different approach to determination of critical density and corrections for faint galaxies. The final percentage of group members ($\sim 65\%$) is similar to the NBG. Six of the observed galaxies appeared in both lists. One galaxy which appeared only in the Fouqué list (NGC 2640) was also observed, but not included in the final analysis due to reduction problems.

The final selection of galaxies was also dependent on the time of year allocated for observing.

The properties of the galaxies presented are listed in Table 2. The columns of Table 2 contain the following information: (1) Name of galaxy, (2) and (3) galaxy coordinates, (4) RSA/CA Hubble type, (5) RC3 Hubble type (6) the total, face-on blue magnitude from deVaucouleurs *et al.* (1991), (7) the heliocentric radial velocity, (8) the distance of the galaxy in Mpc, based on the heliocentric velocity and the multiattractor model for the velocity fields within the Local Supercluster (Tonry *et al.* 2000; Masters, K. L., private communication), with an assumed Hubble constant of $70 \text{ km s}^{-1} \text{ Mpc}^{-1}$, (9) A_R , scaled from A_B values listed in deVaucouleurs *et al.* (1991) using values given in Riefe & Lebofsky (1985), (10) the HI deficiency parameter, as defined by Solanes *et al.* (1996; see also Giovanelli & Haynes 1983), (11) the local galaxy density in units of galaxies Mpc^{-3} , given in the NBG, and (12) the affiliation of a galaxy with respect to associations, as defined by the NBG: ‘at-large’ means the galaxy is unassociated with other galaxies within the large scale cloud, ‘association’ means that the galaxy is associated with other galaxies within the cloud. The HI

TABLE 1
COMPLETENESS OF OBSERVED ISOLATED SAMPLE

Hubble Type	RSA		RC3	
	$M_B \leq -19$	$-19 < M_B \leq -18$	$M_B \leq -19$	$-19 < M_B \leq -18$
S0-S0/a	50% (4/8)	100% (1/1)	36% (4/11)	50% (1/2)
Sa-Sab	44% (4/9)	- (0/0)	60% (9/15)	0% (0/1)
Sb-Sbc	27% (6/22)	33% (1/3)	19% (5/26)	13% (1/8)
Sc-Scd	21% (7/34)	22% (2/9)	15% (6/41)	18% (2/11)
Total (all)	29% (21/73)	11% (4/13)	26% (24/93)	18% (4/22)
Total (Sa-Scd)	26% (17/65)	18% (3/12)	24% (20/82)	15% (3/20)
Total (all mags)	29% (25/86) ^a	-	24% (28/115) ^b	-
Total (Sa-Scd)	26% (20/77)	-	23% (23/102)	-

NOTE. — Completeness of the observed isolated sample given as percentages and ratios of observed to total. The following selection criteria were used to extract candidate galaxies from the NBG catalog: no group members, $v_{he} < 2500 \text{ km s}^{-1}$, distance $< 33 \text{ Mpc}$, NBG local density $< 0.3 \text{ gal Mpc}^{-3}$, inclination $< 75^\circ$. Completeness is given as a function of both RSA and RC3 morphological types. Absolute magnitudes are derived from distances given by NBG.

^aThe total number is 25 rather than 29 because four galaxies were not listed in the RSA catalog.

^bThe total number is 28 rather than 29 because one galaxy classified as Sc by RSA was classified as Sm by RC3.

fluxes used to extract the HI deficiencies in column (10) were extracted from the Cornell University Extragalactic Group private digital HI archive, and are corrected for effects such as beam dilution (Springob *et al.* 2005; see also Haynes & Giovanelli 1984), while optical diameters were obtained from the Arecibo General Catalog, a private database maintained at Cornell University by Martha Haynes and Riccardo Giovanelli.

Both the RC3 and RSA classes are listed in Table 2. (Note that the agreement between classifiers is far better for this isolated sample of galaxies than for galaxies listed in the Virgo Cluster sample of Koopmann *et al.* 2001).

3. OBSERVATIONS AND REDUCTIONS

The observations of the isolated galaxies were made on the KPNO 0.9-m and the CTIO 0.9-m and 1.5-m telescopes on photometric nights between August 1993 and February 1996. Exposures ranged from 3-15 min in a standard Harris (Kron-Cousins) R filter, and 1-2 hrs in an H α filter of width 60-80 \AA , centered either near 6573 \AA or near 6600 \AA (for galaxies with $v > 1000 \text{ km/s}$). An observing log is presented in Table 3. Galaxies are listed in order by right ascension, with two to three lines describing the R and H α observations. The columns list the following information: (1) name of the galaxy, (2) the date of the observation, (3) the telescope and chip in column 3 (where chip characteristics are given in Table 4), (4) filter (where filter codes and characteristics are given in Table 5), (5) exposure time in seconds, (6) airmass of the observation, (7) the full width half maximum (FWHM) in arcseconds, (8) the sky background sigma, (9) and the estimated uncertainty in the sky level. The units of columns (8) and (9) are $\text{erg cm}^{-2}\text{s}^{-1}\text{arcsec}^{-2}$. The values for the R observations may be converted to magnitudes using a zeropoint of 13.945.

The absolute flux calibration was based on observations of the spectrophotometric standard stars from the lists of Massey *et al.* (1988) and Hamuy *et al.* (1992). Landolt (1992) standards were observed to derive the extinction coefficient and/or monitor the photometricity, and in some cases, to calibrate the observations.

Reduction procedures were identical to those described

in Koopmann *et al.* (2001). Multiple exposures were registered and combined. Images were flux calibrated to the Massey *et al.* (1988) and Hamuy *et al.* (1992) spectrophotometric standards. The sky background was subtracted from the R and H α images before continuum subtraction. Uncertainties in the sky levels were typically 0.5-1% for R and 1-2% for H α , as listed in Column (9) of Table 3. The continuum light was subtracted from the H α image using a scaled R image. A full discussion of the uncertainties in the continuum subtraction is provided in Koopmann *et al.* (2001).

As in previous papers in the series, no correction was made for contamination by the 2 [NII] lines ($\lambda \lambda=6548.1, 6583.8 \text{ \AA}$) that also lie within the H α filter bandpass. The ratio of [NII] to H α flux in HII regions has been estimated by Kennicutt (1992) to be 0.53 in the median. It appears to be dependent upon galaxy luminosity (e.g., Jansen *et al.* 2000) such that fainter galaxies have a smaller [NII] contamination. See also James *et al.* (2005) for a complete literature review. James *et al.* (2005) probe the radial dependence of the [NII]/H α correction factor using narrow-band H α and [NII] imaging of 7 spiral galaxies. They find lower values for the global [N II]/H α ratio than previous studies and show that the value has a strong dependence on radius. The value and the radial dependence vary widely in their small sample. One Sc galaxy, for example, has no detectable [NII] emission. The value and radial dependence of [NII]/H α are sources of uncertainty in our fluxes and surface photometry. If the James *et al.* galaxies are typical, the contribution from [NII] is most significant in nuclear regions, meaning that our profiles tend to be too bright at inner radii. However, without detailed knowledge of the value of N II]/H α as a function of radius, we do not attempt a correction. Hereafter we will abbreviate H α +[NII] as H α .

The H α fluxes were not corrected for the presence of the H α emission line in the R continuum image, in order to be consistent with fluxes given in Koopmann *et al.* (2001) and Young *et al.* 1996. This correction amounts to a factor of 4-5% depending on the H α filter used.

These isolated sample galaxies are located at many dif-

FIG. 1.— The R and H α images and surface photometry. Galaxies are ordered according to right ascension. The images are displayed on a log scale, with north up and east to the left. The tickmarks on the images are spaced by 1.0 arcmin, and the solid line on each image represents 1 arcmin, with the corresponding scale in kpc given for each galaxy. Sky around some of the larger field-of-view images was cropped; refer to Tables 3 and 4 for the actual size of the image frames. The RSA/CA morphology class is noted in the righthand corner of the R image and the RSA/CA and RC3 morphological types are indicated in the surface photometry plots. In the surface photometry plots, the R (solid) and H α (dotted) profiles are plotted as a function of radius in arc seconds. The H α profiles were superposed using an arbitrary zeropoint of 18.945. A solid line indicating 1 kpc is provided below the morphological types. The isophotal radius at 24 mag arcsec $^{-2}$, r_{24} and the disk scalelength, r_d , are indicated with arrows. An error bar for the R profile is given at r_{24} , and the R profile ends where the noise becomes greater than the signal. The H α profile is cut at the radius of the outermost HII region. Diamonds on the H α profile indicate annuli for which the sky uncertainty was greater than the azimuthally averaged signal. The solid dot on the H α profile is plotted at the 17×10^{-18} isophotal radius.

ferent galactic latitudes and it was necessary to apply a correction for galactic extinction. Absorption values in the B filter listed in the RC3 were scaled to R and H α using the values given in Rieke & Lebofsky (1985). A_R values are listed in Column (9) of Table 2.

4. ATLAS OF ISOLATED GALAXIES

R and H α images and surface photometry of the 29 isolated galaxies are presented in Figure 1. Galaxies are ordered by right ascension, with morphological information and size scales indicated on the plots. In the left-hand column, the images are displayed on a log scale, with north up and east to the left. In the righthand column, R (solid) and H α (dotted) surface photometry profiles are plotted as a function of radius in arc seconds. The H α profiles are displaced from the R profiles using an arbitrary zeropoint of 18.945. The H α profile is plotted out to the radius containing the outermost resolved HII region. Radial parameters derived from the surface photometry (as described in Section 4.1) are indicated in the plots, as explained in the figure caption.

4.1. Surface Photometry

Surface brightness profiles were obtained from the images using a surface photometry program written in the IDL programming language. The full procedure is described in Koopmann *et al.* (2001); this section presents a brief summary of the approach.

The center of the galaxy was derived using centroiding via the *center* task in IRAF. The axial ratio and position angle were derived from fitting to the outer isophotes. The center, axial ratio, and position angle were held fixed in the determination of the profile.

The R radial profiles were calculated until the error in the sky background exceeded the signal. The H α surface photometry was halted just outside the radius of the outermost HII region. For galaxies with faint outer disk star formation or galaxies with scattered background light or poor flat fields, this radius was beyond the point in the profile where sky uncertainty errors overwhelmed the azimuthally averaged signal. We indicate this radius in the plots of radial profiles given in Figure 1, but plot the H α radial profile to the outermost HII region to emphasize the extent of star formation.

All profiles were corrected to face on assuming complete transparency in the disk (see discussion in Koopmann *et al.* 2001). Profiles of individual galaxies are plotted in the right-hand columns of Figure 1. The H α profiles were arbitrarily scaled to the R profile using a zeropoint of 18.945. The morphological type of each galaxy is indicated.

The main contributor of noise in the radial profile is the uncertainty in the sky level. There are several other systematic errors which have not been included in the error bars. The error in the flux calibration contributes $\sim 5\%$. In H α , systematic errors due to the continuum subtraction and contribution of [N II] are typically 20-30%. See Figure 7 of Koopmann *et al.* (2001) for a graphical example of the uncertainty in the H α surface photometry.

Table 6 presents quantities derived from the R surface photometry. The columns provide: (1) Name of galaxy, (2) axial ratio and, in parentheses, inclination calculated using the Hubble (1926) conversion (see Koopmann *et al.* 2001), (3) position angle, (4) r_{24} , the radius in units of arcsecs at the 24 R mag/arcsec 2 isophote, (5) the magnitude within r_{24} , (6) r_{25} , the radius in units of arcsecs at the 25 R mag/arcsec 2 isophote, (7) the magnitude within r_{25} , (8) the central R light concentration parameter, (9) the disk scalelength, and (10) the uncertainty in the disk scalelength, including axial ratios, position angles, isophotal radii and magnitudes, and disk scalelengths. The central R light concentration parameter given in Column (8) is defined analogously to Abraham *et al.* (1994), as

$$C30 = \frac{F_R(0.3r_{24})}{F_R(r_{24})}$$

where $F_R(r_{24})$ is the flux in R measured within the r_{24} isophote and $F_R(0.3r_{24})$ is the flux within the $0.3r_{24}$ isophote.

Table 7 presents quantities derived from the H α surface photometry. The information listed in the columns is: (1) Name of galaxy, (2) log of the total H α flux in units of 10^{-18} erg cm $^{-2}$ s $^{-1}$, with uncertainty based on the background sky error combined in quadrature with an estimated 3% error in the continuum subtraction factor, (3) H α equivalent width in Å, as defined below, with uncertainty, (4) semimajor radius in arcseconds of the outermost HII region, (5) radius in arcseconds which contains 95% of the total H α flux, (6) radius in arcseconds at which the surface brightness falls to 17×10^{-18} erg cm $^{-2}$ s $^{-1}$ arcsec $^{-2}$, (7) log of the H α flux within $r_{H\alpha 17}$ in units of 1×10^{-18} erg cm $^{-2}$ s $^{-1}$, and (8) the H α concentration, as defined below.

The H α equivalent width given in Column (3) was derived from the H α and R photometry via the formula

$$EW = \frac{F_{H\alpha}}{kF_R} \delta\lambda,$$

where F_R is the R flux, k is the scaling factor used in the continuum subtraction (typically 0.04-0.05), and $\delta\lambda$ is the width of the H α filter in Å. A linear fit to the H α equivalent width and the NMSFR parameter produces:

$$EW = 1476(\pm 83) \left(\frac{F_{H\alpha}}{F_R(r_{24})} \right)$$

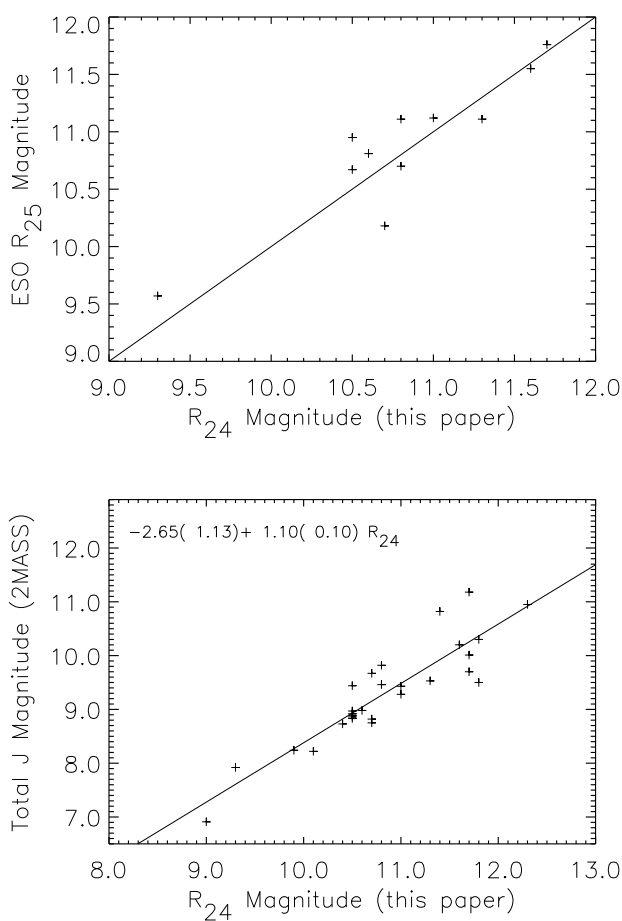


FIG. 2.— The R photometry given in this paper is correlated with other sources of photometry. (a) Comparison of isophotal R magnitudes given in this paper and in Lauberts & Valentijn (1989), for 11 galaxies in common. The solid line shows a one-to-one correlation. The scatter in a best-fit line is 15%. (b) Comparison between our isophotal R magnitudes and 2MASS total J magnitudes. The solid line shows a linear least-squares fit to the data. The equation of the line is given in the plot. The scatter in the fit is 10%.

Column (8) of Table 7 provides the H α light concentration parameter, defined as

$$CH\alpha = \frac{F_{H\alpha}(0.3r_{24})}{F_{H\alpha}},$$

where $F_{H\alpha}$ is the total H α flux and $F_{H\alpha}(0.3r_{24})$ is the flux within the $0.3r_{24}$ isophote. A $CH\alpha$ of 1 indicates that all of the H α emission is located within $0.3r_{24}$.

5. COMPARISONS TO OTHER SOURCES OF PHOTOMETRY

5.1. Broadband R

Few previous photometric measurements at red wavelengths exist for this set of spirals. Lauberts & Valentijn (1989) contains isophotal magnitudes for 11 galaxies in common. These magnitudes are correlated with our magnitudes, as shown in Figure 2a. The solid line indicates a one-to-one matching. The scatter in a least-squares fit is 15%.

20 of our galaxies have V magnitudes listed in the RC3, and these magnitudes are correlated with our isophotal

R magnitudes with a scatter of about 12%. Eleven of our sample galaxies have been observed in I-band by Haynes *et al.* (private communication). We find a 12% scatter between the R and I photometry. All the sample galaxies have been observed by 2MASS. Total and isophotal J magnitudes were extracted from the 2MASS archive using the Large Galaxy Atlas (Jarrett *et al.* 2003) where possible. Figure 2b shows the correlation between our R magnitudes and the total J magnitude from 2MASS. The scatter in the best-fit line is 10%. (A similar scatter is seen in comparisons of the ESO catalog R and 2MASS J photometry.) The correlation is similar to that obtained using our Virgo Cluster sample galaxies (Koopmann *et al.* 2001), although the Virgo Cluster spirals show somewhat less scatter (7%). Results are similar when isophotal J magnitudes are used in place of the total J magnitudes.

While the scatter in the least-square fits are similar for all 4 comparison bands, we see few galaxies with consistently bright or faint values. Three galaxies show trends in at least 3 bands: our photometry of IC 5273 falls consistently below the trend line compared to other bands, while NGC 3705 and NGC 986 fall consistently above.

5.2. H α

H α fluxes have been measured previously for 10 galaxies, as compiled by Kennicutt & Akiyama (in prep.) and generously provided to us in advance of publication. Kennicutt & Akiyama have placed the H α fluxes of approximately 2600 galaxies in the literature on the same scale, correcting for systematic factors such as broad- vs narrow-band continuum filters and [N II] contamination, and finding average fluxes for galaxies with multiple measurements. The comparison between the scaled literature fluxes and our fluxes is shown in Figure 3. References for the literature values can be found in Kennicutt & Akiyama. To place our fluxes on the same scale as Kennicutt & Akiyama, the galactic extinction correction factor was removed and a 5% correction factor was added to account for the presence of the H α line emission in the R filter. In the plot, galaxies with one literature measurement are represented by cross symbols, while galaxies with two literature measurements are represented by solid circles (NGC 7098) and asterisks (UGC 3580). There is general agreement in the fluxes, although our fluxes may be systematically smaller. On the other hand, H α fluxes from different sources can differ by far more than the internal errors, as seen for the two galaxies with two literature measurements.

6. SUMMARY

Broadband-R and H α images, surface photometry, and quantitative parameters describing central concentrations and star formation rates have been obtained for a sample of 29 isolated S0-Scd spiral galaxies. Further analyses of the spacial distribution of star formation in these galaxies are provided in several papers. The properties of these galaxies are quantitatively compared to those of Virgo Cluster galaxies in Koopmann & Kenney (1998; 2004a; 2004b). H α scale lengths are presented and compared to Virgo Cluster and other field galaxies in Koopmann, Haynes, & Catinella (2005).

The funding for the research on the Virgo cluster and

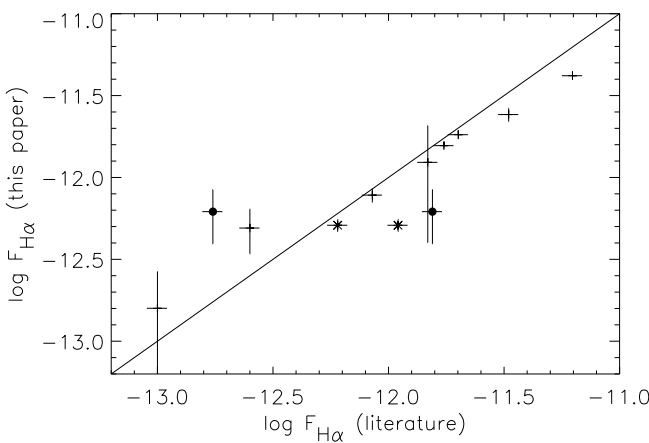


FIG. 3.— The H α photometry given in this paper compared with literature sources as compiled by Kennicutt & Akiyama (in prep). Our H α fluxes were placed on the same scale as Kennicutt & Akiyama, by removing the galactic extinction correction factor and adding an estimated 5% correction factor to account for the presence of the H α line emission in the R filter. The solid line shows a one-to-one correlation. Error bars on the H α photometry in this paper are derived from the sky error combined in quadrature with an estimate of a 3% error in the continuum subtraction factor. Even a 3% error in the continuum subtraction factor can result in a large error in the H α flux for galaxies with relatively weak H α emission, as seen for two galaxies (from left to right, NGC 5273 and IC 356). Kennicutt & Akiyama estimate a typical error in literature values of 5–15%; the error bars shown in the plot are at the 10% level. Cross symbols show those galaxies with one literature measurement. Differences between authors can be much larger than estimated errors, as seen for two galaxies with two measurements in the literature: NGC 7098 (solid circles) and UGC 3580 (asterisks).

isolated spiral galaxies was provided by NSF grant AST-9322779. We thank R.B. Tully for providing us with the online version of the Nearby Galaxies Catalog and software to access it, P. Fouqué for providing us with a list of isolated galaxies, and R. Pogge for excellent advice on obtaining the best continuum subtractions. We are grateful to Sydney Barnes, Shardha Jogee, Jerry Orosz, Sally Cersosimo, and Charles Bailyn for obtaining many of the images in this paper during Yale service observing runs. This work was substantially aided by observing support from the Kitt Peak and Cerro Tololo staffs. Martha Haynes, Christopher Springob, Karen Masters, and the Cornell Extragalactic Group are gratefully acknowledged for their aid in derivation of updated distances and HI deficiencies. This publication makes use of data products from the Two Micron All Sky Survey, which is a joint project of the University of Massachusetts and the Infrared Processing and Analysis Center/California Institute of Technology, funded by the National Aeronautics and Space Administration and the National Science Foundation. This research has made use of the NASA/IPAC Extragalactic Database (NED) which is operated by the Jet Propulsion Laboratory, California Institute of Technology, under contract with the National Aeronautics and Space Administration. The authors and maintainers of the IRAF and STSDAS software packages and instruction manuals are also gratefully acknowledged.

REFERENCES

Abraham, R. G., Valdes, F., Yee, H. K. C., & van den Bergh, S. 1994, ApJ, 432, 75

Allam, S. S., Tucker, D. L., Lee, B. C., & Smith, J. A. 2005, AJ, 129, 2062

deVaucouleurs, G., deVaucouleurs, A., Corwin, H. G., Buta, R. J., Paturel, G., & Fouqué, P. 1991, Third Reference Catalog of Bright Galaxies (New York: Springer-Verlag) (RC3)

Fouqué, P., Gourgoulhon, E., Chamaraux, P., & Paturel, G. 1992, A&AS, 93, 211

Giovanelli, R. & Haynes, M. P. 1983, AJ, 88, 881

Gourgoulhon, E., Chamaraux, P., & Fouqué, P. 1992, A&A, 255, 69

Hamuy, M., Walker, A. R., Suntzeff, N. B., Gigoux, P., Heathcote, S. R., & Phillips, M. M. 1992, PASP, 104, 533

Haynes, M. P. & Giovanelli, R. 1984, AJ, 89, 758

James, P. A., Shane, N. S., Knapen, J. H., Etherton, J., & Percival, S. M. 2005, A&A, 429, 851

Jansen, R. A., Fabricant, D., Franx, M., & Caldwell, N. 2000, ApJS, 126, 331

Jarrett, T. H., Chester, T., Cutri, R., Scheider, S. E., & Huchra, J. P. 2003, AJ, 125, 525

Karachentseva, V. E. 1973, Soobshch. Spets. Astrofiz. Obs., 8, 3

Kennicutt, R. C. 1992, ApJ, 388, 310

Koopmann, R. A., Haynes, M. P., & Catinella, B. 2005, AJ, submitted

Koopmann, R. A. & Kenney, J.D.P. 1998, ApJ, 497, L75

Koopmann, R. A. & Kenney, J.D.P. 2004a, ApJ, 613, 851

Koopmann, R. A. & Kenney, J.D.P. 2004b, ApJ, 613, 866

Koopmann, R. A., Kenney, J. D. P., Young, J. 2001, ApJS, 135, 125

Landolt, A. U. 1992, AJ, 104, 340 (PI)

Lauberts, A. & Valentijn, E. A. 1989, The Surface Photometry Catalogue of the ESO-Uppsala Galaxies (Garching: ESO)

Massey, P., Strobel, K., Barnes, J. V., & Anderson, E. 1988, ApJ, 328, 315

Pisano, D. J., Wilcots, E. M., & Liu, C. T. 2002, ApJS, 142, 161

Poggianti, B. 2005, in Baryons in Dark Matter Halos, R.J. Dettmar, U. Klein, P. Salucci (ed), astro-ph/0503218

Rieke, G. H. & Lebofsky, M. J. 1985, ApJ, 288, 618

Sandage, A., & Bedke, J. 1994, The Carnegie Atlas of Galaxies (Washington: Carnegie)

Sandage, A., & Tammann, G. A. 1987, A Revised Shapley-Ames Catalog of Bright Galaxies (Washington, DC: Carnegie Institution)

Solanes, J. M., Giovanelli, R., & Haynes, M. P. 1996, ApJ, 461, 609

Solanes, J. M., Manrique, A., Garcia-Gomez, C., Gonzalez-Casado, G., Giovanelli, R., & Haynes, M. P. 2001, ApJ, 548, 97

Springob, C. M., Haynes, M. P., Giovanelli, R., & Kent, B. R. 2005, ApJS, in press

Tonry, J. L., Blakeslee, J. P., Ajhar, E. A., & Dressler, A. 2000, ApJ, 530, 625

Tully, R. B. 1987a, Nearby Galaxies Catalog, (Cambridge: Cambridge University Press)

Tully, R. B. 1987b, ApJ, 321, 280

Tully, R. B. 1988, AJ, 96, 73

Vettolani, G., de Souza, R., & Chincarini, G. 1986, A&A, 154, 343

York, D. G., et al. 2000, AJ, 120, 1579

TABLE 2
PROPERTIES OF OBSERVED ISOLATED GALAXIES

Name (1)	RA (2000) (h m s) (2)	Dec (2000) (d m s) (3)	RSA/CA (4)	RC3 (5)	B_T^O (6)	v_{he} (km s $^{-1}$) (7)	Dist (Mpc) (8)	Ext (A_B) (9)	HI Def (10)	ρ_{NBG} (gal Mpc $^{-3}$) (11)	NBG Affil (12)
NGC 578	01 30 29.1	-22 40 03	Sc(s)II	SAB(rs)c	11.17	1630	26.2	.02	.17	0.07	at-large
NGC 613 ^a	01 34 17.4	-29 24 58	SBb(rs)II	SB(rs)bc	10.53	1475	23.9	.02	.40	0.07	at-large
NGC 986	02 33 34.2	-39 02 40	SBb(rs)I-II	SB(rs)ab	11.45	2005	32.2	.03	.58	0.06	at-large
NGC 1249	03 10 06.4	-53 20 17	SBc	SB(s)cd	11.64	1072	17.4	0	.03	0.27	at-large
IC 356	04 07 46.5	+69 48 45	-	SA(s)ab pec	10.17	895	14.6	1.2	-.17	0.08	association
NGC 2090	05 47 02.3	-34 15 05	Sc(s)II	SA(rs)c	11.45	931	15.6	0	-.15	0.14	association
NGC 2196	06 12 09.5	-21 48 23	Sab(s)I	SA(s)ab	11.38	2321	26.8	.45	.31	0.10	association
UGC 3580 ^a	06 55 31.0	+69 33 49	-	SA(s)a pec:	12.20	1201	18.7	.19	.10	0.08	at-large
NGC 2525 ^a	08 05 37.9	-11 25 40	SBc(s)II	SB(s)c	11.55	1581	25.5	.40	.45	0.06	at-large
NGC 2712	08 59 30.6	+44 54 51	SBb(s)I-II	SB(r)b:	12.19	1815	26.4	.04	.14	0.17	at-large
NGC 2787 ^a	9 19 18.5	+69 12 12	SB0/a	SB0(r)+	11.61	696	12.0	.17	0.50	0.06	at-large
NGC 2950	9 42 35.1	+58 51 05	RSB0 $\frac{2}{3}$	(R)SB(r)0	11.80	1337	20.1	.03	>1	0.22	at-large
NGC 3329	10 44 39.5	+76 48 34	Sab	(R)SA(r)b:	12.57	1812	27.2	.03	-	0.20	association
NGC 3359	10 46 36.5	+63 13 24	SBc(s)I.8 pec	SB(rs)c	10.68	1013	16.0	0	-.13	0.21	at-large
NGC 3414	10 51 16.2	+27 58 30	S0 $\frac{1}{2}$ (0)/a	S0pec	11.86	1414	21.4	0	1.1	0.28	association
NGC 3673	11 25 12.7	-26 44 11	SBb(rs)I-II	SB(rs)b	11.81	1938	31.6	.27	.46	.15	association
NGC 3705	11 30 07.6	+09 16 36	Sb(r)I-II	SAB(r)ab	11.25	1017	16.5	.12	.67	0.27	association
NGC 3887 ^a	11 47 04.8	-16 51 16	SBbc(s)II-III	SB(r)bc	11.19	1209	20.2	.05	.03	0.08	at-large
NGC 3941	11 52 55.3	+36 59 11	SB0 $\frac{1}{2}$ /a	SB(s)0	11.25	928	14.6	0	.40	0.29	association
NGC 4597	12 40 12.8	-05 47 59	SBc(r)III:	SB(rs)m	12.21	1043	17.4	.03	-.08	0.19	at-large
NGC 4800	12 54 37.7	+46 31 51	Sb(rs)II-III	SA(rs)b	12.13	891	14.1	0	.28	0.17	at-large
NGC 4984	13 08 57.2	-15 30 59	Sa(s)	(R)SAB(rs)0+	12.03	1206	20.1	.07	1.1	0.26	at-large
NGC 5273	13 42 08.3	+35 39 15	S0/a	SA(s)0	12.38	1054	16.3	0	>1	0.15	association
NGC 5334 ^a	13 52 54.4	-01 06 52	SBc(rs)II	SB(rs)c:	11.62	1383	22.2	0.15	.40	0.16	at-large
NGC 5669	14 32 43.8	+09 53 29	SBc(s)II	SAB(rs)cd	11.79	1371	21.6	.02	.17	0.29	at-large
NGC 7098	21 44 15.4	-75 06 44	-	(R)SAB(rs)a	11.63	2357	37.5	.40	.29	0.07	at-large
NGC 7141	21 52 14.1	-55 34 10	-	SAB(rs)bc	12.21	2978	47.7	0	-	0.18	at-large
IC 5240	22 41 52.3	-44 46 04	SBa(r)	SB(r)a	12.29	1777	29.8	0	.48	0.18	at-large
IC 5273	22 59 26.5	-37 42 12	SBc(s)II-III	SB(rs)cd:	11.55	1301	22.3	.04	.08	0.21	at-large

^aGalaxy also in Fouqué list

TABLE 3
ISOLATED GALAXIES OBSERVING LOG

Name (1)	Date (2)	Telescope/Chip (3)	Filter		Exposure		X (8)	FWHM arcmin (10)	σ_b (11)	H α (12)	δs		
			R (4)	H α (5)	R (6)	H α (7)					R (13)	H α (14)	
NGC 578	1994 Aug 18	CT9/TEK2K	R	H α 6	2 x 450	3 x 2400	1.01	1.01	1.8	530	63	188	2
NGC 613	1992 Aug 18	CT9/TEK1K	R	...	300	...	1.11	...	1.7	1420	...	438	...
	1992 Aug 17	CT9/TEK1K	...	H α 6	...	3 x 2400	...	1.04	1.7	...	138	...	4
NGC 986	1994 Aug 14	CT9/TEK2K	R	H α 6	450	3 x 2400	1.11	1.05	1.5	313	50	188	4
NGC 1249	1992 Aug 20	CT9/TEK1K	R	H α 6	600	5 x 1200	1.17	1.14	1.1	640	56	188	4
IC 356	1995 Feb 06	KP9/t2ka	R	H α 3	3 x 300	3 x 1500	1.27	1.29	1.4	410	43	432	2
NGC 2090	1993 Mar 01	CT9/TEK2K	R	H α 5	900	3 x 2400	1.33	1.05	1.6	525	30	188	4
NGC 2196	1995 Mar 03	CT15/TEK1K	R	H α 6	4 x 90	4 x 600	1.30	1.17	1.6	380	27	135	3
UGC 3580	1995 Feb 02	KP9/t2ka	R	H α 3	2 x 450	3 x 1800	1.29	1.27	1.4	162	50	65	2
NGC 2525	1994 Feb 24	CT9/TEK2K	R	H α 6	3 x 450	3 x 2400	1.07	1.06	1.6	593	143	310	4
NGC 2712	1995 Feb 03	KP9/t2ka	R	H α 4	2 x 450	3 x 1200	1.15	1.10	1.5	164	50	65	3
NGC 2787	1995 Feb 03	KP9/t2ka	R	H α 3	4 x 150	3 x 1500	1.66	1.56	1.6	302	26	108	3
NGC 2950	1995 Feb 04	KP9/t2ka	R	H α 3	5 x 72	3 x 900	1.29	1.24	1.6	260	30	65	4
NGC 3329	1995 Feb 02	KP9/t2ka	R	H α 4	2 x 300	3 x 1800	1.51	1.47	1.5	260	21	65	2
NGC 3359	1995 Feb 05	KP9/t2ka	R	H α 3	2 x 450	3 x 1200	1.51	1.43	1.4	310	10	65	2
NGC 3414	1995 Feb 06	KP9/t2ka	R	H α 4	5 x 120	3 x 900	1.37	1.25	1.6	260	20	108	3
NGC 3673	1995 Mar 29	CT15/TEK1K	R	H α 6	4 x 90	4 x 600	1.11	1.09	1.5	350	27	81	3
NGC 3705	1995 Feb 03	KP9/t2ka	R	H α 3	4 x 70	4 x 900	1.44	1.44	1.4	390	32	43	1
NGC 3887	1994 Feb 25	CT9/TEK2K	R	H α 6	2 x 450	3 x 2400	1.16	1.09	2.6	535	90	128	4
NGC 3941	1995 Feb 04	KP9/t2ka	R	H α 3	5 x 75	4 x 750	1.43	1.32	1.4	280	26	130	4
NGC 4597	1993 Mar 02	CT9/TEK1K	R	H α 6	900	3 x 2400	1.18	1.13	1.7	421	45	64	2
NGC 4800	1995 Feb 06	KP9/t2ka	R	H α 3	3 x 240	4 x 900	1.05	1.03	1.2	151	22	65	2
NGC 4984	1993 Mar 01	CT9/TEK2K	R	H α 6	450	3 x 2400	1.13	1.04	2.0	287	38	128	4
NGC 5273	1995 Feb 04	KP9/t2ka	R	H α 3	3 x 300	3 x 1200	1.01	1.00	1.4	91	20	43	3
NGC 5334	1995 Mar 29	CT15/Tek1K	R	H α 6	4 x 90	4 x 600	1.67	1.57	1.1	310	22	216	3
NGC 5669	1995 Feb 05	KP9/t2ka	R	H α 3	2 x 450	3 x 1200	1.14	1.11	1.2	182	24	65	2
NGC 7098	1994 Aug 15	CT9/TEK2K	R	H α 6	2 x 450	3 x 2400	1.43	1.44	2.2	216	51	255	5
NGC 7141	1994 Aug 13	CT9/TEK2K	R	H α 6	2 x 450	3 x 2400	1.26	1.35	1.7	264	64	319	5
IC 5240	1994 Aug 12	CT9/TEK2K	R	H α 6	2 x 450	3 x 2400	1.10	1.18	1.7	160	51	160	5
IC 5273	1992 Aug 18	CT9/TEK1K	R	H α 6	300	3 x 2400	1.40	1.07	2.0	1500	115	574	5

TABLE 4
CHIP CODES AND CHARACTERISTICS

Detector	Scale ($''$ pix $^{-1}$)	Size (pix)	FOV ($''$)
t2ka	0.68	2048	23.2
TEK2K	0.40	2048	13.7
TEK1K	0.40	1024	6.8

TABLE 5
FILTER
CHARACTERISTICS

Filter	λ_{cent} (Å)	$\delta\lambda$ (Å)
H α 3	6573	68
H α 4	6618	74
H α 5	6563	78
H α 6	6606	75
R	6425	1540

TABLE 6
PARAMETERS AND DERIVED QUANTITIES FOR THE R SURFACE PHOTOMETRY

Name	Inc ($^{\circ}$)	PA ($^{\circ}$)	r ₂₄ ($''$)	R ₂₄ (mag)	r ₂₅ ($''$)	R ₂₅ (mag)	C30	r _d ($''$)	Δ r _d ($''$)
(1)	(2)	(3)	(4)	(5)	(6)	(7)	(8)	(9)	(10)
NGC 578	0.574 (57)	110	117	10.8	146	10.7	0.36	35	3
NGC 613	0.799 (38)	120	207	9.3	0	0.0	0.44	63	3
NGC 986	0.743 (43)	150	119	10.7	144	10.6	0.49	38	3
NGC 1249	0.500 (62)	85	94	11.6	121	11.5	0.32	40	3
IC 356	0.719 (45)	105 ^a	252	9.0	0	0.0	0.52	81	10
NGC 2090	0.484 (63)	13	99	10.5	173	10.4	0.50	-	-
NGC 2196	0.682 (48) ^a	53 ^a	102	10.6	140	10.5	0.54	31	5
UGC 3580	0.469 (64)	5	60	12.3	90	12.1	0.49	28	3
NGC 2525	0.643 (51)	75	100	10.7	118	10.7	0.30	30	5
NGC 2712	0.500 (62)	0	64	11.7	86	11.7	0.37	19	2
NGC 2787	0.574 (57)	130 ^a	104	10.1	129	10.0	0.61	25	3
NGC 2950	0.656 (50)	127 ^a	93	10.5	113	10.5	0.73	26	2
NGC 3329	0.559 (58)	133 ^a	55	11.8	77	11.8	0.58	20	3
NGC 3359	0.643 (51)	175	142	10.5	184	10.4	0.37	43	2
NGC 3414	0.839 (34) ^a	30	104	10.5	149	10.5	0.61	-	-
NGC 3673	0.500 (62) ^a	75	109	11.0	139	11.0	0.41	33	3
NGC 3705	0.423 (68)	119	112	10.7	146	10.6	0.35	32	2
NGC 3887	0.766 (41)	19	109	10.5	130	10.4	0.40	27	3
NGC 3941	0.731 (44) ^a	10	98	9.9	119	9.9	0.65	22	2
NGC 4597	0.423 (68)	49	93	12.0	120	11.8	0.21	40	6
NGC 4800	0.766 (41)	25	60	11.0	78	11.0	0.56	19	5
NGC 4984	0.755 (42)	15 ^a	115	10.4	159	10.3	0.65	40	4
NGC 5273	0.866 (31)	10	68	11.8	84	11.7	0.42	20	3
NGC 5334	0.719 (45)	15	101	11.4	126	11.3	0.27	40	4
NGC 5669	0.707 (46)	50	90	11.7	117	11.5	0.34	31	4
NGC 7098	0.574 (57)	70	135	10.5	162	10.5	0.57	42	4
NGC 7141	0.707 (46)	0 ^a	77	11.7	124	11.5	0.39	32	4
IC 5240	0.643 (51)	100	80	11.3	99	11.3	0.49	24	3
IC 5273	0.602 (55)	56	102	10.8	0	0.0	0.35	31	2

^aValue different by more than 5 $^{\circ}$ from RC3.

TABLE 7
PARAMETERS AND DERIVED QUANTITIES FROM THE H α SURFACE PHOTOMETRY

Name	log F _{Hα}	H α EW (\AA)	r _{HII} ($''$)	r _{Hα95} ($''$)	r _{Hα17} ($''$)	log F _{Hα17}	CH α
(1)	(2)	(3)	(4)	(5)	(6)	(7)	(8)
NGC 578	-11.52 \pm 0.03	36 \pm 2	135	104	102	-11.54	0.25
NGC 613	-11.34 \pm 0.09	14 \pm 2	164	101	113	-11.34	0.60
NGC 986	-11.63 \pm 0.04	23 \pm 2	108	82	91	-11.63	0.49
NGC 1249	-11.76 \pm 0.03	39 \pm 3	179	137	80	-11.85	0.25
IC 356	-11.66 \pm 0.17	5 \pm 2	245	184	150	-11.73	0.29
NGC 2090	-11.58 \pm 0.04	31 \pm 2	287	203	122	-11.73	0.32
NGC 2196	-11.74 \pm 0.06	16 \pm 2	123	112	99	-11.80	0.18
UGC 3580	-12.27 \pm 0.04	25 \pm 2	130	100	35	-12.40	0.63
NGC 2525	-11.49 \pm 0.03	35 \pm 3	88	69	79	-11.49	0.20
NGC 2712	-12.12 \pm 0.04	23 \pm 2	98	69	59	-12.17	0.27
NGC 2787	-13.14 \pm 0.7	0.5 \pm 2	31	27	13	-13.31	1.00
NGC 2950	-12.59 \pm 0.5	3 \pm 2	49	44	31	-12.69	0.76
NGC 3329	-12.33 \pm 0.06	13 \pm 2	63	53	34	-12.42	0.43
NGC 3359	-11.40 \pm 0.02	12 \pm 2	235	176	141	-11.46	0.24
NGC 3414	-12.89 \pm 0.4	1 \pm 2	33	28	19	-13.00	0.99
NGC 3673	-12.09 \pm 0.09	11 \pm 2	139	124	73	-12.29	0.13
NGC 3705	-11.69 \pm 0.04	24 \pm 2	196	141	96	-11.77	0.23
NGC 3887	-11.36 \pm 0.03	39 \pm 3	125	100	108	-11.38	0.17
NGC 3941	-12.50 \pm 0.3	2 \pm 2	94	87	17	-13.07	0.31
NGC 4597	-11.82 \pm 0.02	48 \pm 3	149	123	106	-11.87	0.07
NGC 4800	-11.89 \pm 0.04	20 \pm 2	58	40	45	-11.90	0.54
NGC 4984	-11.99 \pm 0.11	8 \pm 2	50	35	41	-12.00	0.94
NGC 5273	-12.82 \pm 0.4	3 \pm 2	10	3	6	-12.82	0.45
NGC 5334	-11.82 \pm 0.04	27 \pm 2	131	115	102	-11.89	0.16
NGC 5669	-11.82 \pm 0.02	42 \pm 2	138	115	113	-11.84	0.23
NGC 7098	-12.14 \pm 0.14	7 \pm 2	137	126	66	-12.41	0.25
NGC 7141	-12.28 \pm 0.08	13 \pm 2	126	114	64	-12.43	0.35
IC 5240	-12.33 \pm 0.14	7 \pm 2	88	79	60	-12.47	0.10
IC 5273	-11.77 \pm 0.06	7 \pm 2	89	60	70	-11.77	0.38

This figure "f1a.jpg" is available in "jpg" format from:

<http://arxiv.org/ps/astro-ph/0511665v1>

This figure "f1b.jpg" is available in "jpg" format from:

<http://arxiv.org/ps/astro-ph/0511665v1>

This figure "f1c.jpg" is available in "jpg" format from:

<http://arxiv.org/ps/astro-ph/0511665v1>

This figure "f1d.jpg" is available in "jpg" format from:

<http://arxiv.org/ps/astro-ph/0511665v1>

This figure "f1e.jpg" is available in "jpg" format from:

<http://arxiv.org/ps/astro-ph/0511665v1>

This figure "f1f.jpg" is available in "jpg" format from:

<http://arxiv.org/ps/astro-ph/0511665v1>

This figure "f1g.jpg" is available in "jpg" format from:

<http://arxiv.org/ps/astro-ph/0511665v1>

This figure "f1h.jpg" is available in "jpg" format from:

<http://arxiv.org/ps/astro-ph/0511665v1>